JACS
JOURNAL OF THE AMERICAN CHEMICAL SOCIETY
Article
pubs.acs.org/JACS

Molecules–Oligomers–Nanowires–Graphene Nanoribbons: A Bottom-Up Stepwise On-Surface Covalent Synthesis Preserving Long-Range Order

Andrea Basagni,*[,†] Francesco Sedona,*[,†] Carlo A. Pignedoli,[‡] Mattia Cattelan,[†] Louis Nicolas,[§,†] Maurizio Casarin,[†] and Mauro Sambi[†]

[†]Dipartimento di Scienze Chimiche, Università degli Studi di Padova and Consorzio INSTM, Via Marzolo 1, 35131 Padova, Italy
[‡]NCCR MARVEL, Empa, Swiss Federal Laboratories for Materials Science and Technology, nanotech@surfaces laboratory, 8600 Dübendorf, Switzerland
[§]Ecole Normale Supérieure de Cachan 61, avenue du Président Wilson, 94235 Cachan cedex, France

Supporting Information

ABSTRACT: We report on a stepwise on-surface polymerization reaction leading to oriented graphene nanoribbons on Au(111) as the final product. Starting from the precursor 4,4″-dibromo-*p*-terphenyl and using the Ullmann coupling reaction followed by dehydrogenation and C–C coupling, we have developed a fine-tuned, annealing-triggered on-surface polymerization that allows us to obtain an oriented nanomesh of graphene nanoribbons via two well-defined intermediate products, namely, *p*-phenylene oligomers with reduced length dispersion and ordered submicrometric molecular wires of poly(*p*-phenylene). A fine balance involving gold catalytic activity in the Ullmann coupling, appropriate on-surface molecular mobility, and favorable topochemical conditions provided by the used precursor leads to a high degree of long-range order that characterizes each step of the synthesis and is rarely observed for surface organic frameworks obtained via Ullmann coupling.

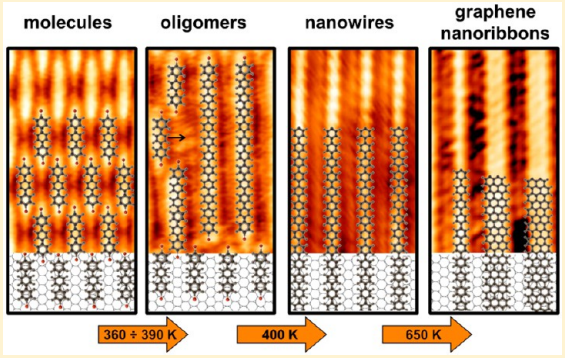

INTRODUCTION

In the last years, the research interests in the field of surface-supported organic monolayers have been focused on two main topics: the growth of epitaxial graphene and the production of surface covalent organic frameworks (SCOFs).[1−8]

Since graphene layers on metal surfaces represent the global thermodynamic minimum of all conjugated carbon allotropes, simple on-surface thermal decomposition of hydrocarbons[9] or surface segregation of carbon-containing alloys[10] are becoming the methods of choice to prepare large-area graphene films on various transition-metal surfaces. At the same time, the absence of a band gap in graphene, which is required in order to implement it as a component in field-effect transistor (FET) devices,[11,12] has stimulated the development of "defective" graphene-like materials by means of chemical modification,[13,14] defects engineering,[15,16] and confinement of charge carriers within quasi-one-dimensional (1D) ribbons[11,17] or quantum nanodots.[18]

The versatility of organic functionalization has directed research toward the bottom-up synthesis of graphene-like structures, with the aim of inserting functional groups in the starting building units to tailor the properties at one's own choice.[19−21] However, well-ordered SCOFs are rarely obtained under ultrahigh-vacuum conditions[22−24] because several local thermodynamic minima can be reached starting from a selected precursor.[25] For this reason, the degree of order in a bidimensional covalent layer can be improved only by careful control of the reaction kinetics.[25−27]

To date, one of the most successful meeting points between the two mentioned research areas has been the precise production of graphene nanoribbons (GNRs) and hetero-junctions starting from the precursor 10,10′-dibromo-9,9′-bianthryl (DBBA) or similar molecules.[28−30] In addition, several other molecular building blocks have been tested to obtain "defective" graphene-like materials, but with less impressive results due to the difficulty of obtaining large regular domains.[31−34]

Herein we propose a novel finely tuned annealing protocol to perform a stepwise on-surface polymerization reaction leading to oriented GNRs as the final product. In particular, GNRs can be grown using 4,4″-dibromo-*p*-terphenyl (DBTP) as the precursor according to the mechanism shown in Figure 1. On Au(111), the first step is the Ullmann coupling between brominated precursor units[35−40] in order to form ordered and extended poly(*p*-phenylene) (PPP) wires, which subsequently act as precursors for the synthesis of GNRs after C–H bond activation.[41−46]

Received: October 7, 2014
Published: January 13, 2015

DOI: 10.1021/ja510292b
J. Am. Chem. Soc. 2015, 137, 1802−1808

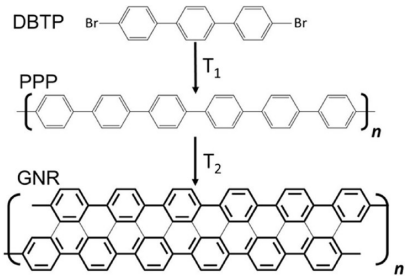

Figure 1. Schematic representation of the bottom-up synthesis of GNRs from the precursor DBTP.

This new approach allowed us to fine-tune the degree of polymerization by controlling the annealing temperature and, if required, to stop the synthesis at a particular intermediate prior to the formation of GNRs, namely, *p*-phenylene oligomers with reduced length dispersion or submicrometric molecular wires of PPP. Moreover, a higher annealing temperature promoted the formation of an oriented nanomesh of GNRs. As a result of the close match between the self-assembled structure of the as-deposited DBTP molecules and the motif of PPP wires, short-range molecular displacements lead from the starting structure to the final structure with no need for long-range on-surface diffusion. Basically for this reason every intermediate product of the synthesis is characterized by extended 2D order, which leads to oriented growth of GNRs with their main axes mostly parallel to the substrate main directions.

RESULTS AND DISCUSSION

The models and experimental scanning tunneling microscopy (STM) images in Figure 2 summarize the main steps in the synthesis of GNRs starting from DBTP, along with the structural features of every intermediate ordered nanostructure. Larger STM images are reported in Figure 3 for the same structures in order to show the extended bidimensional order and the behavior of the herringbone (HB) Au(111) surface reconstruction underneath the reacting molecular layer.

The deposition of a submonolayer of DBTP at room temperature (RT) on Au(111) results in an ordered, close-packed array of unreacted monomers, as shown in Figures 2a and 3a, where molecules can be clearly resolved as linear features oriented with their main axes parallel to the $[1\bar{2}1]$ substrate direction. RT X-ray photoelectron spectroscopy (XPS) outcomes ultimately indicate that the molecules are intact when they adsorb on the surface. Indeed, the C 1s peak (Figure 4d) is characterized by a major component at a binding energy (BE) of 284.2 eV, associated with the phenyl ring, and a smaller feature at BE = 285.1 eV due to bromine-bonded carbon atoms.[47] Consistent with nondissociative adsorption of DBTP, as observed for similar halogenated molecules on Au(111),[26,47−51] the stoichiometric ratio (SR) of the two components is 1:8. This is further supported by the Br 3d spectra, which reveal the presence of carbon-bonded bromine only (Br $3d_{5/2}$ at BE = 69.9 eV; Figure 4a), with no detectable trace of chemisorbed atomic bromine.[48,49] This close-packed self-assembled structure, described by the [3 1, 2.5 5.5] matrix (see the low-energy electron diffraction (LEED) pattern in Figure S1a in the Supporting Information), is stabilized by lateral Br···H−C hydrogen bonds and Br···Br X bonds, as sketched in the inset of Figure 2a and in line with other recently described brominated molecules.[51,52]

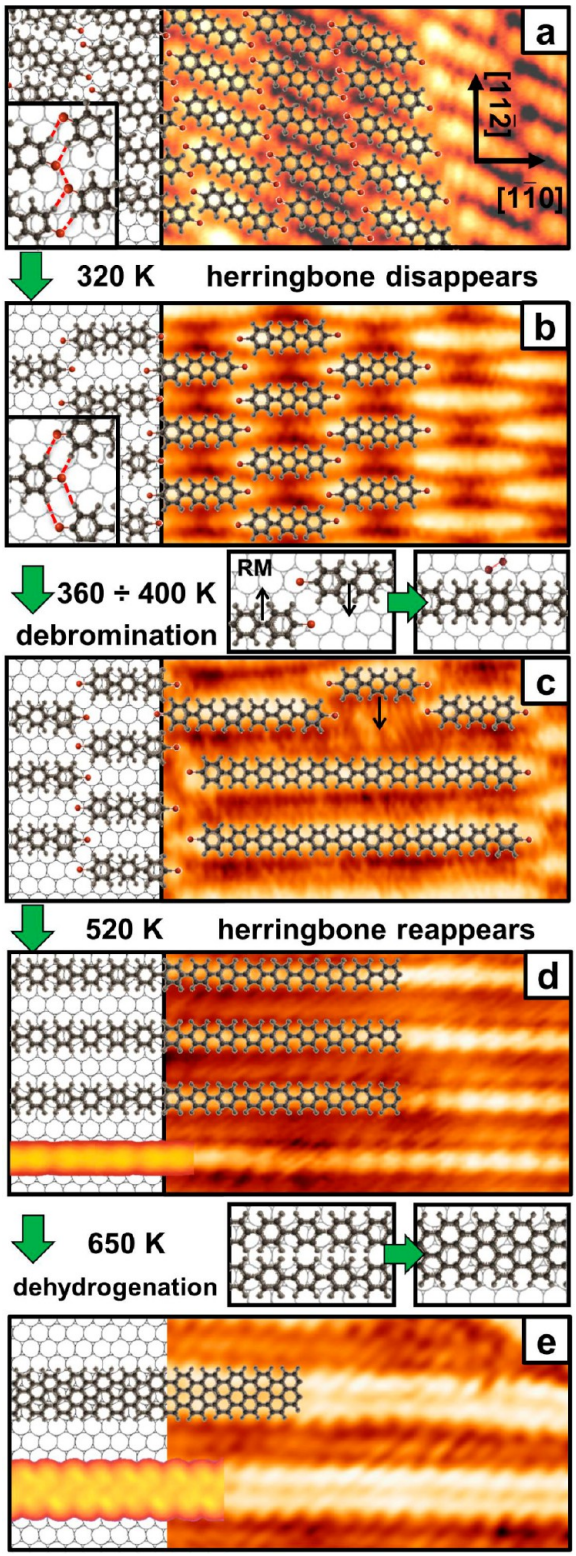

Figure 2. Diagrammatic representation of the different structures obtained during the synthesis of GNRs. For each reaction step, the annealing temperature and the main structural and chemical effects on the system are indicated. All of the images are aligned as reported in (a). The bottom left insets in panels (d) and (e) report DFT-based STM simulations ($V = -0.4$ V) of the PPP wire and a GNR with $N = 6$, respectively, for comparison with the experimental images.

After postdeposition annealing of the structure reported in Figure 2a to 320 K, the network is converted into the less dense

DOI: 10.1021/ja510292b
J. Am. Chem. Soc. 2015, 137, 1802−1808

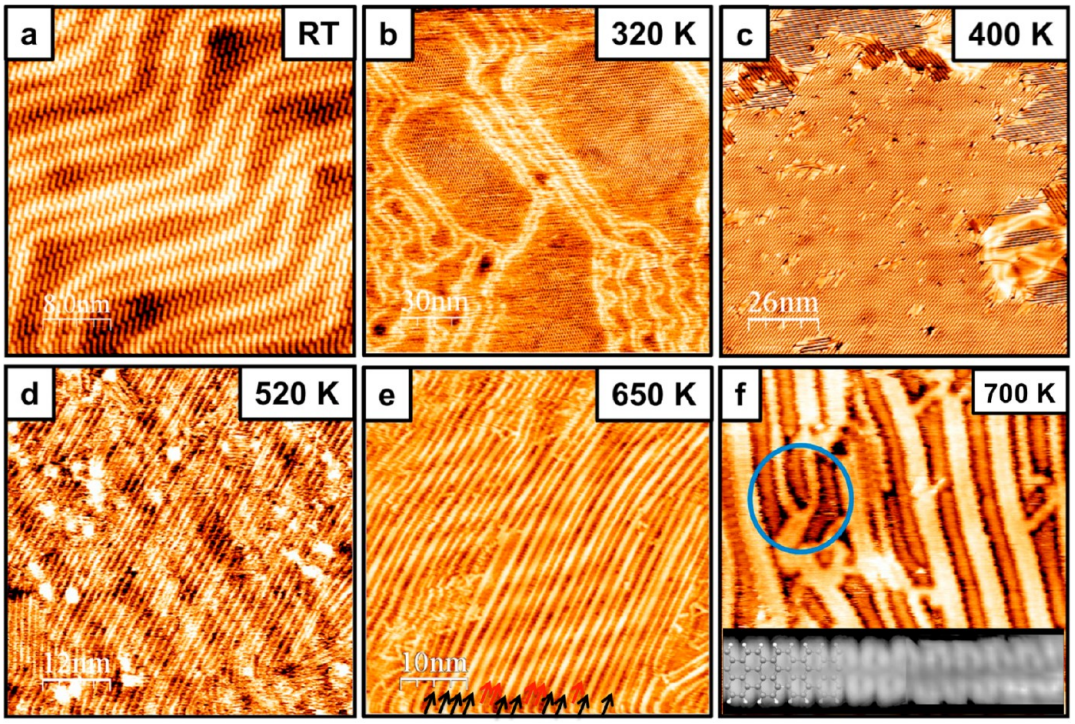

Figure 3. STM images of the Au(111) surface after each thermal treatment step, evidencing the range of the bidimensional order and the behavior of the Au(111) HB surface reconstruction. (a) Molecules deposited at RT. The HB is clearly visible underneath the molecules. (b) After annealing at 320 K, the HB disappears beneath the [4 2, 2 6] structure and is visible only on the uncovered areas. (c) After annealing at 400 K, long PPP wires are formed, and the HB is still visible only on the uncovered areas. (d) After annealing at 520 K, PPP wires have a more wavy geometry, and the HB reappears under the molecules. (e) After annealing at 650 K, parallel GNRs (black arrows) are formed from the PPP wires (red arrows). (f) The blue circle highlights two PPP wires extending from the head of a GNR. The bottom inset reports a comparison between a DFT-based simulation (V = −0.7 V) with a partially superimposed molecular model (left) and an experimental high-resolution STM image (V = −0.7 V, I = 1 nA) (right) of a GNR with N = 6.

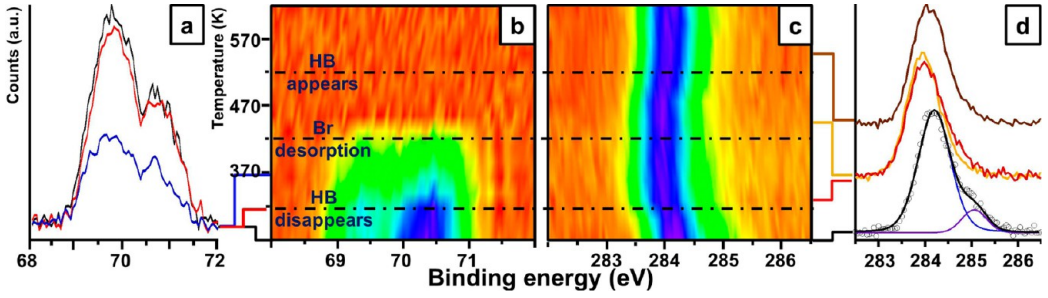

Figure 4. (a, b) Br 3d and (c, d) C 1s X-ray photoelectron spectra as functions of temperature for DBTP/Au(111). The three dash-dotted lines correspond to the onset temperatures for herringbone (HB) reconstruction lifting, bromine desorption, and HB reappearance. Selected spectra acquired at different temperatures are shown in (a) for Br 3d and in (d) for C 1s.

[4 2, 2 6] structure (see the LEED pattern in Figure S1b), where the molecules lie parallel to the [1$\bar{1}$0] direction, as shown in Figure 2b. Moreover, direct comparison of panels (a) and (b) in Figure 3 shows that at RT the Au(111) HB reconstruction is visible under the molecules, while it disappears underneath the new phase after the annealing. Figure 4 shows that the C 1s XPS peak is the only one affected by this phase transition, with a 0.3 eV shift toward lower BE, while the Br 3d doublet retains its initial position and area. Since at this temperature the chemical identity of DBTP molecules is preserved, we associate the bright protrusions clearly visible at the head and tail of each molecule (Figure 2b) to Br atoms. To confirm this conclusion, we simulated the STM images of the [4 2, 2 6] structure by assuming both the brominated molecule and the debrominated biradical (Figure S2), and we concluded that only the first choice matches the experimental images.

In a recent spectroscopic study of the Ullmann coupling reaction of DBBA on Au(111),[48] a similar C 1s shift was associated with dehalogenation of the molecules as a result of the concurrent shift of Br-related peaks at BE values compatible with the presence of chemisorbed bromine atoms on the surface. In our case, the C 1s shift cannot be associated with any change in the Br 3d XPS peak. For this reason, we propose that the new superstructure is not related to a chemical reaction but rather to a different vertical interaction between the DBTP molecules and the substrate. Indeed, the RT nanostructure is very compact, and the nearest-neighbor intermolecular H−H distance is compatible only with partially tilted molecules; in the lower-density phase, however, molecules can lie flat on the

DOI: 10.1021/ja510292b
J. Am. Chem. Soc. 2015, 137, 1802−1808

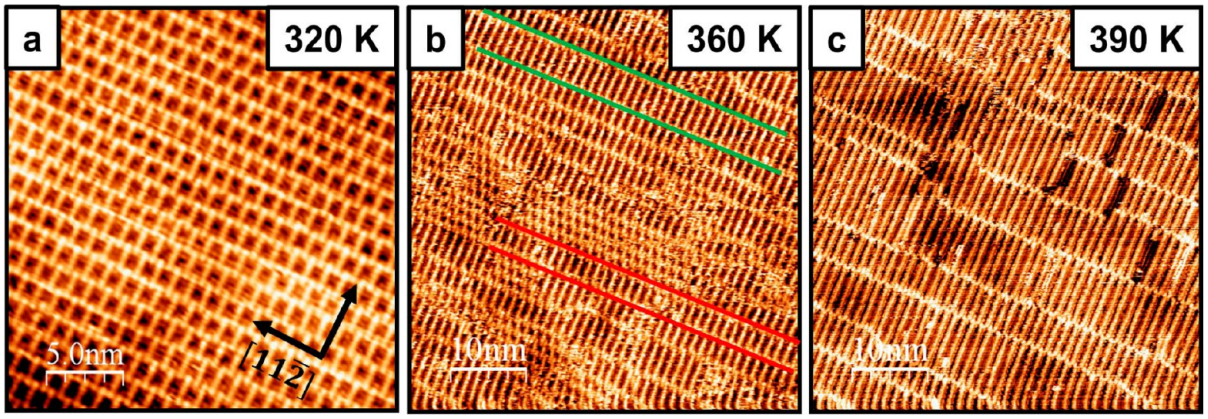

Figure 5. STM images of the self-assembled structures formed by (a) monomers and (b, c) oligomers after annealing at different temperatures, as indicated for each image. Same-length oligomers form rows parallel to the [11$\bar{2}$] direction, as highlighted by the red and green segments in (b) for dimers and trimers, respectively.

surface, and the local lifting of the HB reconstruction appears to be due to adsorbate-induced stress, similar to what is observed for polycyclic aromatic hydrocarbons adsorbed on the same surface.[53,54]

Further annealing at temperatures ranging between 360 and 390 K promotes the formation of longer oligomolecular units, as shown in Figures 2c and 5. Since these molecules are slightly shorter than an integer multiple of the individual monomers and appear with a uniform height profile, we conclude that they are oligomers of *p*-phenylene such as dimers, trimers, tetramers, and so on (see Figure S3). As sketched by the arrow in Figure 2c, the DBTP molecules in the [4 2, 2 6] structure are properly aligned to form oligomers by a little sliding motion along the [11$\bar{2}$] direction, associated with the elimination of a bromine molecule and the concurrent formation of a C−C bond. Indeed, during this step the area of the Br 3d doublet decreases monotonically as a function of temperature without the formation of chemisorbed bromine atoms (Figure 4a,b), and at the same time the C 1s peak becomes more symmetric. In particular, the decrease in the higher-BE side is associated with the increase in the lower-BE side, in accordance with the formation of new C−C bonds at the expense of the C−Br ones (see the superposition of the red and yellow spectra in Figure 4d).

As shown in Figure 5b, oligomers of the same length form rows along the [11$\bar{2}$] direction (isolated oligomers are rarely observed). This observation implies that a shift of a DBTP molecule along the [11$\bar{2}$] direction leads to coupling between units along the molecular main axis, and this movement in turn favors a cooperative shift of all of the subsequent molecules in the same [11$\bar{2}$]-aligned row as a consequence of the increased steric hindrance between nearest neighbors due to Pauli repulsion, according to the typical Sergeant−Soldier mechanism. Moreover, careful control of the surface temperature between 360 and 390 K promotes the formation of longer oligomers such as heptamers, octamers, and so on (see the statistical analysis reported in Figure S4).

Increasing the temperature over 400 K results in a network of PPP wires characterized by unprecedented long-range order, as confirmed by the presence of the well-defined LEED pattern shown in Figure S1c, which was previously unreported for on-surface Ullmann-produced polymers and is compatible with a commensurate [4 2, 0 3] structure. The dimensions of the PPP wires are limited only by the grain boundaries of the islands, as shown in Figure 3c, and can reach 200 nm, even if typical values are around 70 nm. The PPP wires are stable up to 650 K, but an important change shows up after the annealing at 520 K: above this temperature the overlayer LEED pattern disappears, and STM imaging revealed that the molecular wires acquire a more wavy geometry, with the contextual restoration of the HB reconstruction underneath the molecular layer (Figure 3d). At the same annealing temperature, we observed a 0.2 eV shift in the C 1s XPS peak toward higher BE, as visible in Figure 4c,d. Again, there is an evident correlation between the C 1s shift and the restoration of the HB reconstruction, at variance with recent spectroscopic studies of similar systems[48] that revealed a correlation between this second C 1s shift and the complete desorption of bromine, which in our case is completed at distinctly lower temperatures, as reported in Figure 4b.

We next explored the carbon−carbon coupling reaction through direct C−H activation in order to achieve the side coupling between adjacent PPP wires. After the treatment at 650 K, we observed the formation of wider molecular stripes, mainly oriented parallel to the PPP wires (see Figures 2e and 3e) and having the same apparent height. A closer inspection of the STM images reveals the presence of some branches arising from the stripe structures. In particular, it appears that some ribbons split into two distinct branches, both having the same shape and dimensions of a single PPP wire, as highlighted in Figure 3f. We conclude that the wider nanostructures formed after thermal annealing at 650 K are GNRs. Our conclusion is further supported by a comparison of the high-resolution STM images reported in Figures 2e and 3f with density functional theory (DFT) simulations obtained by assuming the formation of an armchair GNR with $N = 6$, as expected for the condensation of two PPP wires (see Figure 1) but a novel geometry with respect to GNRs obtained previously by means of on-surface synthesis.[28,46] In detail, the simulated images show that the edge is characterized by an antiphase zigzag domain boundary, a feature revealed by STM imaging. Moreover, Raman spectra (see Figure S5) conclusively demonstrate the formation of GNRs, since the G′, D + D′, and 2G bands, which are very sensitive fingerprints of the presence of graphenic materials,[55,56] show up after annealing at 650 K. Although the dispersion of the lengths is large, ranging from 10 to 70 nm, this reaction protocol affords mostly aligned GNRs, as is evident in Figure 3e. Almost all of the nanoribbons terminate in one or two wires as a result of nonperfect zipping

DOI: 10.1021/ja510292b
J. Am. Chem. Soc. 2015, 137, 1802−1808

of two PPP molecules. This leads to nanoribbons serially connected by PPP wires.

Annealing at temperatures near the threshold for C−H bond activation (650 K) mainly promotes the coupling of two PPP wires, while treatments at higher temperatures (up to 800 K) activate the condensation of unreacted wires, leading to wider GNRs, as shown by the STM image reported in Figure 6a.

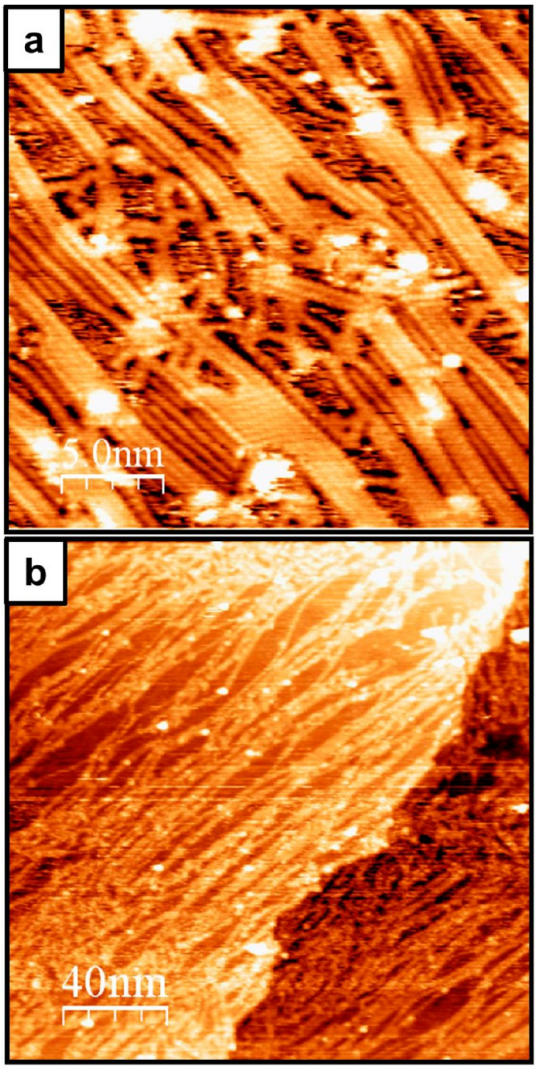

Figure 6. (a) STM image of wider GNRs due to the coupling of more than two PPP wires prepared after annealing PPP wires at 800 K. (b) Large-scale image showing the preferential azimuthal orientation of the defective GNR mesh.

However, this reaction step is not driven by self-assembly any more, but rather by long-range, random diffusional events activated by the high temperature. For this reason, the coupling between aryl groups occurs randomly, leading to the formation of branches that interconnect the nanoribbons; the resulting structure is a sort of highly defective GNR mesh in which a clear preferential azimuthal orientation deriving from the hierarchical procedure is still evident (see Figure 6b).

CONCLUSIONS

We have reported a bottom-up synthesis of submicron-length, long-range-ordered PPP as an intermediate product and large, oriented graphene nanoribbons as the final product using 4,4″-dibromo-*p*-terphenyl as the molecular precursor on Au(111). Moreover, fine-tuning of the reaction conditions allows the degree of polymerization in the Ullmann coupling reaction to be controlled with almost monomolecular precision.

The comparison of results reported here with those obtained by Lin and co-workers[57] on Cu(111) is particularly interesting. On Cu(111), the DBTP self-assembled structure is converted into an organometallic network prior to the formation of PPP wires, and a limited 2D order is obtained. This intermediate is not observed on gold, in agreement with what has been observed previously for other halogenated molecules on the same surface.[50,58,59] In this respect, as inferred by Lackinger and co-workers,[26] the gold surface might still be the best compromise between sufficient catalytic activity, high molecular mobility, and weak adsorption energy for the halogen leaving group. In the present case, gold acts as the catalyst for the Ullmann reaction, but it does not form an organometallic network with the selected debrominated precursor. A direct consequence is that the molecules can self-organize freely, and only when they are properly aligned does the reaction occur, as reported previously in the case of GNRs obtained from the precursor DBBA.[28]

An interesting difference between the cases of GNRs formed from DBBA and from DBTP is the behavior of bromine, as revealed by XPS analysis: in the former case, Br atoms detach from the monomer and adsorb on the Au(111) substrate by annealing between 400 and 500 K and then desorb as Br_2 molecules after annealing at 550 K, whereas when DBTP is used on the same substrate, bromine desorbs in the much lower temperature range of 360−400 K and no adsorbed atomic bromine is detected by XPS.[49] This difference can be easily explained when the different structures formed by the deposited molecules before the debromination step are analyzed. In the case of DBBA, the brominated molecules form ordered rows with the Br atoms relatively far from each other.[59] As a consequence, annealing induces the adsorption of isolated Br atoms on the surface, too far from each other to form Br_2 molecules unless thermal diffusion sets in. Conversely, DBTP molecules arrange in the [4 2, 2 6] structure, where the apical Br atoms residing on nearest-neighbor molecules are close to each other, and therefore, thermally triggered C−Br bond cleavage puts two nearby Br atoms at a mutual bonding distance, thereby promoting the formation and contextual desorption of a Br_2 molecule. Concurrently, with a little sliding motion along the $[11\bar{2}]$ direction, the two remaining radicals can react to form a C−C bond. In summary, in the DBBA case the rate-limiting step for bromine desorption is most likely set by the rate of Br_2 formation as a result of random diffusion of adsorbed atomic Br, whereas in the present case the rate-limiting step appears to be C−Br bond cleavage, with the spatial confinement of Br couples due to the starting geometry favoring almost immediate subsequent formation and desorption of molecular bromine.

As a final remark, this work confirms once more[23] that one of the most efficient ways to obtain large domains of long-range ordered SCOFs using nonreversible covalent coupling, as in the case of Ullmann-type reactions, is to start from a supramolecular arrangement of precursors that is able to rearrange into the final covalent nanostructure with small local positional/orientational adjustments, thus avoiding long-range on-surface diffusion, which typically leads to highly defective final structures. In this way it has been possible to obtain large ordered domains of PPP and GNRs with their main axes mostly

DOI: 10.1021/ja510292b
J. Am. Chem. Soc. 2015, 137, 1802−1808

parallel to the substrate main directions. In perspective, the reported synthesis seems to be the most favorable candidate for the growth of unidirectional and size-controlled ribbons by exploiting a surface templating effect.[60,61] By confining the rodlike molecules onto the reduced-width terrace of a vicinal surface, we expect to achieve both a highly anisotropic material on the macroscopic length scale and fine control of the dimensional dispersion. Moreover, this method is not limited to the synthesis of carbon-rich materials but should be applicable to the introduction of dopant atomic species or functional groups in specific positions if a proper rodlike precursor is employed.

EXPERIMENTAL SECTION

STM Imaging. Experiments were performed under ultrahigh-vacuum conditions at a base pressure of 2×10^{-10} mbar with an Omicron scanning tunneling microscope (VT-STM). All of the STM measurements were carried out at RT in constant-current mode using an electrochemically etched Pt−Ir tip. Typical parameters were a sample bias voltage (V_{bias}) of ±1 V and a tunneling current (I) of 2−5 nA. The STM data were processed with the WSxM software.[62] Moderate filtering was applied for noise reduction.

Sample Preparation. The Au(111) crystal was cleaned by repeated cycles of 1 keV Ar^+ sputtering and annealing at 820 K until a clean surface with sufficiently large terraces was confirmed by STM imaging. Commercially available DBTP molecules were deposited from a pyrolytic boron nitride crucible held at ∼390 K. The coverage was 0.7 monolayer (ML) in all of the experiments, as calibrated on the C 1s XPS signal, where 1 ML is defined as a surface fully covered by the [3 1, 2.5 5.5] structure. The molecular source was outgassed until the pressure did not increase during the sublimation. During deposition the surface was always held at RT, and the polymerization was activated by subsequent thermal annealing. The final temperature was kept for at least 3 h to allow the system to evolve until it reached a stationary state under the given conditions; the samples were then cooled to RT and analyzed. STM images were statistically analyzed by molecular counting. Molecules were only considered when they were completely resolved, and the analysis encompassed at least 3000 molecules for each temperature.

X-ray Photoelectron Spectroscopy. Measurements were performed in situ at RT using a VG Scienta XM 650 X-ray source. The X-rays produced were monochromatized using a VG Scienta XM 780 monochromator optimized for Al Kα radiation (1486.7 eV). Photoelectrons were collected and analyzed with a Scienta SES 100 electron analyzer fitted to the STM preparation chamber.

Simulations. Simulations of DBTP networks adsorbed on the Au(111) surface were performed using DFT in the mixed Gaussian plane waves framework as implemented in the CP2K code.[63] We used the Perdew−Burke−Ernzerhof (PBE) parametrization of the exchange−correlation functional. DFT-D3 dispersion corrections were included.[64]

The Au(111) substrate was modeled within the repeated slab geometry[65] using orthorhombic simulation cells containing four layers of gold and one layer of hydrogen atoms to suppress the surface state of Au(111) on one side of the slab. The lateral size of the unit cell corresponded to 200 unit cells (10 × 10 rectangular units), and more than 20 Å of vacuum was included. The geometries of the topmost two Au(111) layers and the adsorbed molecular species were fully optimized until forces on atoms were lower that 10^{-4} a.u. STM simulations were performed in the Tersoff−Hamann approximation[66] in constant-current mode. To overcome limitations of localized basis sets for nonperiodic systems, the electronic states were extrapolated into the vacuum region.[67] Since the tip shape and the tip−sample distance were not accessible experimentally, a quantitative simulation of the experimental tunneling current was not attempted here. We chose the charge-density isovalue to provide a realistic tip−sample distance on the order of 5 Å.

Raman Spectroscopy. Raman spectra were acquired with a ThermoFisher DXR Raman microscope using a 532 nm laser (3.0 mW) focused on the sample with a 50× objective (Olympus) to obtain a spot size of about 1 μm. A single acquisition lasted no more than 20 min to avoid laser-induced damage of the sample.

ASSOCIATED CONTENT

Supporting Information

Detailed descriptions of experimental procedures, LEED results, simulation of DBTP STM images, STM statistical analysis, and Raman measurements. This material is available free of charge via the Internet at http://pubs.acs.org.

AUTHOR INFORMATION

Corresponding Authors

*andrea.basagni@studenti.unipd.it
*francesco.sedona@unipd.it

Notes

The authors declare no competing financial interest.

ACKNOWLEDGMENTS

This work was partially funded by MIUR (PRIN 2010/11, Project 2010BNZ3F2: "DESCARTES"), Progetti di Ricerca di Ateneo (CPDA118475/11), and Progetto Futuro in Ricerca 2012 (RBFR128BEC). The Swiss Federal Supercomputing Center (CSCS) is acknowledged for computational resources (Project s507).

REFERENCES

(1) Colson, J.; Dichtel, W. *Nat. Chem.* **2013**, *5*, 453−465.
(2) Lafferentz, L.; Eberhardt, V.; Dri, C.; Africh, C.; Comelli, G.; Esch, F.; Hecht, S.; Grill, L. *Nat. Chem.* **2012**, *4*, 215−220.
(3) Sakamoto, J.; van Heijst, J.; Lukin, O.; Schlüter, A. D. *Angew. Chem., Int. Ed.* **2009**, *48*, 1030−1069.
(4) Grill, L.; Dyer, M.; Lafferentz, L.; Persson, M.; Peters, M. V.; Hecht, S. *Nat. Nanotechnol.* **2007**, *2*, 687−691.
(5) Mas-Ballesté, R.; Gómez-Navarro, C.; Gómez-Herrero, J.; Zamora, F. *Nanoscale* **2011**, *3*, 20−30.
(6) Wofford, J. M.; Starodub, E.; Walter, A. L.; Nie, S.; Bostwick, A.; Bartelt, N. C.; Thürmer, K.; Rotenberg, E.; McCarty, K. F.; Dubon, O. D. *New J. Phys.* **2012**, *14*, No. 053008.
(7) Geim, A. K.; Novoselov, K. S. *Nat. Mater.* **2007**, *6*, 183−191.
(8) Seyller, T.; Bostwick, A.; Emtsev, K. V.; Horn, K.; Ley, L.; McChesney, J. L.; Ohta, T.; Riley, J. D.; Rotenberg, E.; Speck, F. *Phys. Status Solidi B* **2008**, *245*, 1436−1446.
(9) Gao, L.; Guest, J. R.; Guisinger, N. P. *Nano Lett.* **2010**, *10*, 3512−3516.
(10) Sutter, P. W.; Flege, J.-I.; Sutter, E. A. *Nat. Mater.* **2008**, *7*, 406−411.
(11) Wang, X.; Ouyang, Y.; Li, X.; Wang, H.; Guo, J.; Dai, H. *Phys. Rev. Lett.* **2008**, *100*, No. 206803.
(12) Lv, R.; Terrones, M. *Mater. Lett.* **2012**, *78*, 209−218.
(13) Elias, D. C.; Nair, R. R.; Mohiuddin, T. M. G.; Morozov, S. V.; Blake, P.; Halsall, M. P.; Ferrari, A. C.; Boukhvalov, D. W.; Katsnelson, M. I.; Geim, A. K.; Novoselov, K. S. *Science* **2009**, *323*, 610−613.
(14) Nair, R. R.; Ren, W.; Jalil, R.; Riaz, I.; Kravets, V. G.; Britnell, L.; Blake, P.; Schedin, F.; Mayorov, A. S.; Yuan, S.; Katsnelson, M. I.; Cheng, H.-M.; Strupinski, W.; Bulusheva, L. G.; Okotrub, A. V.; Grigorieva, I. V.; Grigorenko, A. N.; Novoselov, K. S.; Geim, A. K. *Small* **2010**, *6*, 2877−2884.
(15) Terrones, H.; Lv, R.; Terrones, M.; Dresselhaus, M. S. *Rep. Prog. Phys.* **2012**, *75*, No. 062501.
(16) Banhart, F.; Kotakoski, J.; Krasheninnikov, A. V. *ACS Nano* **2011**, *5*, 26−41.
(17) Yan, Q.; Huang, B.; Yu, J.; Zheng, F.; Zang, J.; Wu, J.; Gu, B.-L.; Liu, F.; Duan, W. *Nano Lett.* **2007**, *7*, 1469−1473.

DOI: 10.1021/ja510292b
J. Am. Chem. Soc. 2015, 137, 1802−1808

(18) Lee, J.; Kim, K.; Park, W. I.; Kim, B.-H.; Park, J. H.; Kim, T.-H.; Bong, S.; Kim, C.-H.; Chae, G.; Jun, M.; Hwang, Y.; Jung, Y. S.; Jeon, S. *Nano Lett.* **2012**, *12*, 6078−6083.
(19) Xu, L.; Zhou, X.; Yu, Y.; Tian, W. Q.; Ma, J.; Lei, S. *ACS Nano* **2013**, *7*, 8066−8073.
(20) Dienstmaier, J. F.; Medina, D. D.; Dogru, M.; Knochel, P.; Bein, T.; Heckl, W. M.; Lackinger, M. *ACS Nano* **2012**, *6*, 7234−7242.
(21) Tanoue, R.; Higuchi, R.; Ikebe, K.; Uemura, S.; Kimizuka, N.; Stieg, A. Z.; Gimzewski, J. K.; Kunitake, M. *J. Electroanal. Chem.* **2014**, *716*, 145−149.
(22) Basagni, A.; Colazzo, L.; Sedona, F.; DiMarino, M.; Carofiglio, T.; Lubian, E.; Forrer, D.; Vittadini, A.; Casarin, M.; Verdini, A.; Cossaro, A.; Floreano, L.; Sambi, M. *Chem.—Eur. J.* **2014**, *20*, 14296−14304.
(23) Sedona, F.; Di Marino, M.; Sambi, M.; Carofiglio, T.; Lubian, E.; Casarin, M.; Tondello, E. *ACS Nano* **2010**, *4*, 5147−5154.
(24) Deshpande, A.; Sham, C.-H.; Alaboson, J. M. P.; Mullin, J. M.; Schatz, G. C.; Hersam, M. C. *J. Am. Chem. Soc.* **2012**, *134*, 16759−16764.
(25) Ourdjini, O.; Pawlak, R.; Abel, M.; Clair, S.; Chen, L.; Bergeon, N.; Sassi, M.; Oison, V.; Debierre, J.-M.; Coratger, R.; Porte, L. *Phys. Rev. B* **2011**, *84*, No. 125421.
(26) Eichhorn, J.; Nieckarz, D.; Ochs, O.; Samanta, D.; Schmittel, M.; Szabelski, P. J.; Lackinger, M. *ACS Nano* **2014**, *8*, 7880−7889.
(27) Eichhorn, J.; Strunskus, T.; Rastgoo-Lahrood, A.; Samanta, D.; Schmittel, M.; Lackinger, M. *Chem. Commun.* **2014**, *50*, 7680−7682.
(28) Cai, J.; Ruffieux, P.; Jaafar, R.; Bieri, M.; Braun, T.; Blankenburg, S.; Muoth, M.; Seitsonen, A. P.; Saleh, M.; Feng, X.; Müllen, K.; Fasel, R. *Nature* **2010**, *466*, 470−473.
(29) Blankenburg, S.; Cai, J.; Ruffieux, P.; Jaafar, R.; Passerone, D.; Feng, X.; Müllen, K.; Fasel, R.; Pignedoli, C. A. *ACS Nano* **2012**, *6*, 2020−2025.
(30) Cai, J.; Pignedoli, C. A.; Talirz, L.; Ruffieux, P.; Söde, H.; Liang, L.; Meunier, V.; Berger, R.; Li, R.; Feng, X.; Müllen, K.; Fasel, R. *Nat. Nanotechnol.* **2014**, *9*, 896−900.
(31) Bieri, M.; Treier, M.; Cai, J.; Aït-Mansour, K.; Ruffieux, P.; Gröning, O.; Gröning, P.; Kastler, M.; Rieger, R.; Feng, X.; Müllen, K.; Fasel, R. *Chem. Commun.* **2009**, 6919−6921.
(32) Fan, Q.; Wang, C.; Liu, L.; Han, Y.; Zhao, J.; Zhu, J.; Kuttner, J.; Hilt, G.; Gottfried, J. M. *J. Phys. Chem. C* **2014**, *118*, 13018−13025.
(33) Gutzler, R.; Walch, H.; Eder, G.; Kloft, S.; Heckl, W. M.; Lackinger, M. *Chem. Commun.* **2009**, 4456−4458.
(34) Bieri, M.; Blankenburg, S.; Kivala, M.; Pignedoli, C. A.; Ruffieux, P.; Müllen, K.; Fasel, R. *Chem. Commun.* **2011**, *47*, 10239−10241.
(35) Fan, Q.; Wang, C.; Han, Y.; Zhu, J.; Hieringer, W.; Kuttner, J.; Hilt, G.; Gottfried, J. M. *Angew. Chem., Int. Ed.* **2013**, *52*, 4668−4672.
(36) Lin, T.; Shang, X. S.; Adisoejoso, J.; Liu, P. N.; Lin, N. *J. Am. Chem. Soc.* **2013**, *135*, 3576−3582.
(37) Krasnikov, S. A.; Doyle, C. M.; Sergeeva, N. N.; Preobrajenski, A. B.; Vinogradov, N. A.; Sergeeva, Y. N.; Zakharov, A. A.; Senge, M. O.; Cafolla, A. A. *Nano Res.* **2011**, *4*, 376−384.
(38) Fan, Q.; Wang, C.; Han, Y.; Zhu, J.; Kuttner, J.; Hilt, G.; Gottfried, J. M. *ACS Nano* **2014**, *8*, 709−718.
(39) Lipton-Duffin, J. A.; Ivasenko, O.; Perepichka, D. F.; Rosei, F. *Small* **2009**, *5*, 592−597.
(40) Di Giovannantonio, M.; El Garah, M.; Lipton-Duffin, J.; Meunier, V.; Cardenas, L.; Fagot Revurat, Y.; Cossaro, A.; Verdini, A.; Perepichka, D. F.; Rosei, F.; Contini, G. *ACS Nano* **2013**, *7*, 8190−8198.
(41) Zhong, D.; Franke, J.-H.; Podiyanachari, S. K.; Blömker, T.; Zhang, H.; Kehr, G.; Erker, G.; Fuchs, H.; Chi, L. *Science* **2011**, *334*, 213−216.
(42) Sun, Q.; Zhang, C.; Kong, H.; Tan, Q.; Xu, W. *Chem. Commun.* **2014**, *50*, 11825−11828.
(43) Müllegger, S.; Winkler, A. *Surf. Sci.* **2006**, *600*, 1290−1299.
(44) In't Veld, M.; Iavicoli, P.; Haq, S.; Amabilino, D. B.; Raval, R. *Chem. Commun.* **2008**, 1536−1538.
(45) Müllegger, S.; Winkler, A. *Surf. Sci.* **2006**, *600*, 3982−3986.
(46) Huang, H.; Wei, D.; Sun, J.; Wong, S. L.; Feng, Y. P.; Neto, A. H. C.; Wee, A. T. S. *Sci. Rep.* **2012**, *2*, No. 983.
(47) Kanuru, V. K.; Kyriakou, G.; Beaumont, S. K.; Papageorgiou, A. C.; Watson, D. J.; Lambert, R. M. *J. Am. Chem. Soc.* **2010**, *132*, 8081−8086.
(48) Batra, A.; Cvetko, D.; Kladnik, G.; Adak, O.; Cardoso, C.; Ferretti, A.; Prezzi, D.; Molinari, E.; Morgante, A.; Venkataraman, L. *Chem. Sci.* **2014**, *5*, 4419−4423.
(49) Simonov, K. A.; Vinogradov, N. A.; Vinogradov, A. S.; Generalov, A. V.; Zagrebina, E. M.; Mårtensson, N.; Cafolla, A. A.; Carpy, T.; Cunniffe, J. P.; Preobrajenski, A. B. *J. Phys. Chem. C* **2014**, *118*, 12532−12540.
(50) Blunt, M. O. M.; Russell, J. J. C.; Champness, N. R.; Beton, P. H. *Chem. Commun.* **2010**, *46*, 7157−7159.
(51) Pham, T. A.; Song, F.; Nguyen, M.-T.; Stöhr, M. *Chem. Commun.* **2014**, *50*, 4−7.
(52) Jang, W. J.; Chung, K.-H.; Lee, M. W.; Kim, H.; Lee, S.; Kahng, S.-J. *Appl. Surf. Sci.* **2014**, *309*, 74−78.
(53) Iski, E. V.; Jewell, A. D.; Tierney, H. L.; Kyriakou, G.; Sykes, E. C. H. *Surf. Sci.* **2012**, *606*, 536−541.
(54) Sellam, F.; Schmitz-Hübsch, T.; Toerker, M. *Surf. Sci.* **2001**, *478*, 113−121.
(55) Dresselhaus, M. S.; Jorio, A.; Hofmann, M.; Dresselhaus, G.; Saito, R. *Nano Lett.* **2010**, *10*, 751−758.
(56) Malard, L. M.; Pimenta, M. A.; Dresselhaus, G.; Dresselhaus, M. S. *Phys. Rep.* **2009**, *473*, 51−87.
(57) Wang, W.; Shi, X.; Wang, S.; Van Hove, M. A.; Lin, N. *J. Am. Chem. Soc.* **2011**, *133*, 13264−13267.
(58) Schlögl, S.; Heckl, W. M.; Lackinger, M. *Surf. Sci.* **2012**, *606*, 999−1004.
(59) Koch, M. Growth and Characterization of Single Molecular Wires on Metal Surfaces. Ph.D. Thesis, Freie Universität Berlin, 2013.
(60) Cirera, B.; Zhang, Y.-Q.; Björk, J.; Klyatskaya, S.; Chen, Z.; Ruben, M.; Barth, J. V.; Klappenberger, F. *Nano Lett.* **2014**, *14*, 1891−1897.
(61) Cañas-Ventura, M. E.; Xiao, W.; Wasserfallen, D.; Müllen, K.; Brune, H.; Barth, J. V.; Fasel, R. *Angew. Chem., Int. Ed.* **2007**, *46*, 1814−1818.
(62) Horcas, I.; Fernández, R.; Gómez-Rodríguez, J. M.; Colchero, J.; Gómez-Herrero, J.; Baro, A. M. *Rev. Sci. Instrum.* **2007**, *78*, No. 013705.
(63) VandeVondele, J.; Krack, M.; Mohamed, F.; Parrinello, M.; Chassaing, T.; Hutter, J. *Comput. Phys. Commun.* **2005**, *167*, 103−128.
(64) Grimme, S.; Antony, J.; Ehrlich, S.; Krieg, H. *J. Chem. Phys.* **2010**, *132*, No. 154104.
(65) Pickett, W. E. *Comput. Phys. Rep.* **1989**, *9*, 115−197.
(66) Tersoff, J.; Hamann, D. *Phys. Rev. B* **1985**, *31*, 805−813.
(67) Tersoff, J. *Phys. Rev. B* **1989**, *40*, 990−993.

DOI: 10.1021/ja510292b
J. Am. Chem. Soc. 2015, 137, 1802−1808